Int J Appl Earth Obs Geoinformation 65 (2018) 124–136

Contents lists available at ScienceDirect

Int J Appl Earth Obs Geoinformation

journal homepage: www.elsevier.com/locate/jag

Research Paper

Retrieval of daily gross primary production over Europe and Africa from an ensemble of SEVIRI/MSG products

B. Martínez[a,*], S. Sanchez-Ruiz[a], M.A. Gilabert[a], A. Moreno[b], M. Campos-Taberner[a], F.J. García-Haro[a], I.F. Trigo[c], M. Aurela[d,1], C. Brümmer[e,1], A. Carrara[f,1], A. De Ligne[g,1], D. Gianelle[h,1], T. Grünwald[i,1], J.M. Limousin[j,1], A. Lohila[k,1], I. Mammarella[l,1], M. Sottocornola[m,1], R. Steinbrecher[n,1], T. Tagesson[o,p,1]

[a] Departament de Física de la Terra i Termodinàmica, Facultat de Física, Universitat de València, Burjassot, Spain
[b] Numerical Terradynamic Simulation Group, University of Montana, Missoula, MT, USA
[c] Instituto Português do Mar e da Atmosfera (IPMA), Lisbon, Portugal
[d] Finnish Meteorological Institute, Helsinki, Finland
[e] Thünen Institute of Climate-Smart Agriculture, Braunschweig, Germany
[f] Fundación Centro de Estudios Ambientales del Mediterráneo (CEAM), Paterna, Spain
[g] TERRA Teaching and Research Centre, Gembloux Agro-Bio Tech, University of Liege, Gembloux, Belgium
[h] Department of Sustainable Agro-Ecosystems and Bioresources, Research and Innovation Center, Fondazione Edmund Mach, Michele all' Adige Trento, Italy
[i] Technische Universität Dresden, Institute of Hydrology and Meteorology, Tharandt, Germany
[j] Centre d'Ecologie Fonctionnelle et Evolutive CEFE, UMR 5175, CNRS–Université de Montpellier–Université Paul Valéry Montpellier–EPHE, Montpellier, France
[k] Finnish Meteorological Institute, Helsinki, Finland
[l] Department of Physics, University of Helsinki, Helsinki, Finland
[m] Department of Science, Waterford Institute of Technology, Waterford, Ireland
[n] Department of Atmospheric Environmental Research, Karlsruhe Institute of Technology, Institute of Meteorology and Climate Research (KIT/IMK–IFU), Garmisch-Partenkirchen, Germany
[o] Department of Physical Geography and Eosystem Sciences, Lund University, Lund, Sweden
[p] Department of Geosciences and Natural Resource Management (IGN), University of Copenhagen, Copenhagen, Denmark

ARTICLE INFO

Keywords:
GPP
MSG
Daily
Water stress
Light-use efficiency
LSA SAF

ABSTRACT

The main goal of this paper is to derive a method for a daily gross primary production (GPP) product over Europe and Africa taking the full advantage of the SEVIRI/MSG satellite products from the European Organization for the Exploitation of Meteorological Satellites (EUMETSAT) sensors delivered from the Satellite Application Facility for Land Surface Analysis (LSA SAF) system. Special attention is paid to model the daily GPP response from an optimized Montheith's light use efficiency model under dry conditions by controlling water shortage limitations from the actual evapotranspiration and the potential evapotranspiration (PET). The PET was parameterized using the mean daily air temperature at 2 m (T_a) from ERA-Interim data. The GPP product (MSG GPP) was produced for 2012 and assessed by direct site-level comparison with GPP from eddy covariance data (EC GPP). MSG GPP presents relative bias errors lower than 40% for the most forest vegetation types with a high agreement ($r > 0.7$) when compared with EC GPP. For drylands, MSG GPP reproduces the seasonal variations related to water limitation in a good agreement with site level GPP estimates (RMSE = 2.11 g m^{-2} day^{-1}; MBE = −0.63 g m^{-2} day^{-1}), especially for the dry season. A consistency analysis against other GPP satellite products (MOD17A2 and FLUXCOM) reveals a high consistency among products (RMSD < 1.5 g m^{-2} day^{-1}) over Europe, North and South Africa. The major GPP disagreement arises over moist biomes in central Africa (RMSD > 3.0 g m^{-2} day^{-1}) and over dry biomes with MSG GPP estimates lower than FLUXCOM (MBD up to −3.0 g m^{-2} day^{-1}). This newly derived product has the potential for analysing spatial patterns and temporal dynamics of GPP at the MSG spatial resolutions on a daily basis allowing to better capture the GPP dynamics and magnitude.

* Corresponding author.
E-mail address: beatriz.martinez@uv.es (B. Martínez).
[1] FLUXNET EC IP.

http://dx.doi.org/10.1016/j.jag.2017.10.011
Received 7 June 2017; Received in revised form 30 October 2017; Accepted 30 October 2017

1. Introduction

Serious concerns associated with climate change are strongly present on the African and European continents leading, among others, to significant effects on plant distribution, growth and productivity (EEA, 2012; IPCC, 2014). Thus, a better understanding of the productivity dynamics of ecosystems across these continents is needed.

Terrestrial ecosystem models provide a powerful tool to integrate our understanding on ecosystem functioning and observations at multiple scales in response to multiple environmental factors (Tian et al., 2010; Yebra et al., 2015). There is a renewed interest in developing carbon flux models that are entirely driven by remotely sensed (RS) observations to estimate gross primary production (GPP) (Running et al., 2004; Gilabert et al., 2015; Tramontana et al., 2016). Estimates of daily GPP (MOD17) (Heinsch et al., 2006; Zhao et al., 2011; Running and Zhao, 2015) are produced operationally for the global terrestrial surface using imagery from the MODerate resolution Imaging Spectroradiometer (MODIS) sensor (Running et al., 2004). Additionally, there clearly is a motivation to extend knowledge acquired from modeling efforts with the MODIS datasets to other sensor's data, such as the Spinning Enhanced Visible and InfraRed Imager (SEVIRI) on board of the Meteosat Second Generation (MSG) platform.

Most of the methodologies for the estimation of GPP from satellite data, such as the widely used MODIS GPP product (Zhao et al., 2011), rely on the well-known satellite-based Production Efficiency Models (PEMs). Most of the PEMs are based on Monteith's light use efficiency (LUE) concept (Monteith, 1972). This concept is still considered to be efficient and widely applicable for the prediction of GPP at different spatial and temporal scales (Waring and Running, 2007) and considers GPP equal to the product of the incoming photosynthetically active radiation (PAR), the fractional absorption of that flux (f_{APAR}) and the light use efficiency (ε). The latter can be operationally parameterized as a function of a maximum value (ε_{max}), which is reduced by different factors related with types of stress that affect the functionality of the plant, such as water availability and thermal stress. These factors range from 0 (total inhibition) to 1 (no inhibition). ε_{max} can be set as invariant across sites and biomes (Myneni et al., 1995) or be derived from biome-dependent values (Garbulsky et al., 2010). According to Schaefer et al. (2012), three areas of the PEMs still need improvements: 1) parameterization of ε_{max}, 2) response function under low temperatures, and 3) GPP response under dry conditions (mainly driven by water stress factors).

In particular, the MODIS standard product parameterizes ε as the product of a biome-specific ε_{max} and the thermal and the water stress factors, which depend on minimum air temperature and vapor pressure deficit, respectively (Zhao et al., 2011; Heinsch et al., 2006). Another parameterization of the water stress based on a water stress coefficient (C_{ws}) has been applied successfully to derive daily GPP estimates in Mediterranean ecosystems (Maselli et al., 2009; Gilabert et al., 2015; Sánchez-Ruiz et al., 2017). C_{ws} accounts for the limited photosynthetic activity in case of short-term water stress from a simplified local water budget based on the ratio of actual evapotranspiration (AET) and potential evapotranspiration (PET). Commonly, evapotranspiration (ET) is normalized by the reference evapotranspiration or by PET in order to characterize water stress (Sepulcre et al., 2014). PET is driven by available energy, while AET reflects an immediate response of vegetation productivity to water-storage (Fisher et al., 2011). Different approaches have been proposed to account for the water stress by means of the AET and PET (Sepulcre et al., 2014; Idso et al., 1981).

The main goal of this paper is to provide a method for the estimation of daily GPP over Europe and Africa from the integration of an ensemble of SEVIRI/MSG products into an optimized LUE model that accounts for water shortage limitations. SEVIRI/MSG satellite products from the European Organization for the Exploitation of Meteorological Satellites (EUMETSAT) sensors delivered from the Satellite Application Facility for Land Surface Analysis (LSA SAF) system are used (http://lsa-saf.eumetsat.int) for 2012. This year is selected due to the unavailability of the necessary inputs for other years. The used set of LSA-SAF products derived from SEVIRI/MSG offers convenient spatial coverage (Europe, Africa and parts of South America) and resolution (Trigo et al., 2011). Moreover, these products are produced operationally in near-real time with generation rates varying from 30 min in the case of ET to daily or 10-day in the case of several vegetation parameters, which makes them particularly suitable for the development of early warning procedures such as drought prediction. Since water availability and radiation are known as main potential climatic constraints to vegetation productivity in many areas of Europe and Africa (Nemani et al., 2003), special attention is paid to capture the GPP response under dry conditions by controlling the water shortage limitations. Thus, a water stress coefficient (C_{ws}) based on the ratio between AET and PET, with PET parameterized using Jensen and Haise (1963), is proposed.

The use of the MSG GPP product can benefit from different aspects. 1) The high quality of the daily down-welling radiation flux (DIDSSF) product (bias and mean absolute error below 6%) confers the MSG GPP estimates of a high reliability. The DIDSSF product is used to compute both the PAR and the C_{ws}, being the PAR the most influential variable in the GPP variance (*e.g.* over 60% of the variance was explained by the PAR in forests over Spain (Gilabert et al., 2015). 2) The daily basis of the MSG GPP product aids, among others, a better characterization of vegetation state and temporal processes (*e.g.* sudden changes from natural hazards or management practices). 3) Clouds effect on the f_{APAR} and DIDSSF is better sampled at daily temporal scale allowing a more accurate characterization as compared to the MODIS product (Heinsch et al., 2006; Gilabert et al., 2015) and also a better understanding of the cloud coverage on the carbon uptake by vegetation.

The performance of the resulting GPP product (MSG GPP) is assessed by site-level comparisons using GPP estimates from eddy covariance (EC) towers. Moreover, the MSG GPP assessment includes consistency analyses against alternative GPP products available from independent remote sensing global data, such as MODIS GPP (MOD17A2) and global flux fields from the Max Planck Institute (MPI) (FLUXCOM) products. The paper first introduces the theoretical basis for the daily GPP retrieval together with the description of the required inputs. The next section describes the MSG GPP assessment and the data used for this purpose. It is followed by a presentation of the obtained results and a discussion section reporting on the differences, advantages and limitations of the MSG GPP retrievals. The main conclusions are presented in the final section.

2. Daily GPP retrieval

The methodology used to derive daily GPP ($g\,m^{-2}\,day^{-1}$) was based on Monteith's LUE approach:

$$GPP = \varepsilon f_{APAR} PAR \quad (1)$$

where

$$\varepsilon = \varepsilon_{max} C_{ws}. \quad (2)$$

Parameter ε was parameterized as ε_{max} downregulated by the water stress coefficient (C_{ws}). Overall, optimized ε_{max} values can range between 0.55–3.5 $g\,MJ^{-1}$, as reported by several authors (Garbulsky et al., 2010; Sjöström et al., 2013; Tagesson et al., 2015). Three values were assigned to the main ecosystems types: 1.8 $g\,MJ^{-1}$ for deciduous broadleaf forest (DBF), 1.5 $g\,MJ^{-1}$ for evergreen needleleaf forest (ENF), and 1.2 $g\,MJ^{-1}$ for remaining ecosystem types (Garbulsky et al., 2010). GPP was not computed for desert areas due to the lack of values for some inputs (*e.g.* DMET) and the high error provided by the f_{APAR} product in these areas.

C_{ws} was parameterized using a variant of the formulation proposed by Maselli et al. (2009):

$$C_{ws} = 0.6 + 0.4\frac{AET}{PET}. \quad (3)$$

Thus, C_{ws} can vary between 0.6 (when water shortage reduces photosynthesis to 60% of its potential value) and 1.0 (when there is no such reduction). This C_{ws} is not as restrictive as the one proposed for Mediterranean ecosystems by Maselli et al. (2009, 2013), in order to reach a compromise between the ability to cope with water limitation during the dry season and the ability to grow at high rates under more favorable water conditions. PET (mm day^{-1}) was parameterized using the Jensen-Haise (JS) empirical equation (Jensen and Haise, 1963):

$$PET = \frac{R_g(0.025T_a + 0.08)}{2450}. \quad (4)$$

Where R_g refers to the daily global irradiation (kJ m^{-2} day^{-1}) and T_a is the daily averaged near-surface air temperature in °C.

The JS method (Eq. (4)) requires only information on climate or meteorological drivers; an important aspect when applying the model on large region scales. The JS approach was originally derived for the semi-arid parts of the United States but is currently used across different climate zones and biomes at the North Dakota Agricultural Weather Network (NDAWN, http://ndawn.ndsu.nodak.edu/) for estimating potential evapotranspiration. It was also successfully applied at regional level over Spain and Italy using MODIS and SPOT-VGT data along with meteorological data to derive an optimized GPP product that accounted for water stress (Maselli et al., 2009; Gilabert et al., 2015).

A subsequent analysis of different water stress parameterizations at EC flux towers in Spain indicated the JS as one of the best methods, explaining 31% and 48% of ε variance in open shrublands and savanna, respectively (Sánchez-Ruiz et al., 2017). The JS approach was also evaluated for two very different sites (one semi-arid savanna grassland and one boreal forest) in the present study, indicating reasonable PET and Cws estimates across various biomes (Fig. S1 in Supplementary material).

The input variables required for the GPP retrieval by means of Eq. (1) are described as follows.

2.1. PAR

PAR is the photosynthetically active radiation in the 0.4–0.7 μm spectral range and was computed as the 46% of daily irradiation (Iqbal, 1983). Daily irradiation images for Europe and Africa provided from the daily down-welling radiation flux (DIDSSF) MSG product (LSA-201) at 3–5 km (depending on the latitude and the distance to nadir view) were used. The DIDSSF product essentially depends on the solar zenith angle, on cloud coverage and, to a lesser extent, on atmospheric absorption and surface albedo (LSA SAF, 2012; Geiger et al., 2008). It is computed by integrating the downward surface solar flux (DSSF) product every 30 min over a whole day. A validation of DSSF using *in situ* data from six European ground measurement stations throughout two years was performed by Geiger et al. (2008). Results show a difference between instantaneous satellite estimates and ground measurements of about 40 and 110 W m^{-2} for clear and cloudy sky conditions, respectively. A more thorough validation of the MSG DSSF product was carried out in Spain (Moreno et al., 2013). The resulting statistics from this validation show a bias of -0.12 MJ m^{-2} (rMBD of about 1%) and a mean absolute difference of 1.0 MJ m^{-2} (rMAD of 6%) in terms of daily global irradiation.

2.2. f_{APAR}

f_{APAR} is the fraction of PAR that is absorbed by leaves and provides a link between the canopy function, *i.e.* its energy absorption capacity, and its structure and condition. The MSG f_{APAR} product (MDFAPAR, LSA-407) delivered by the LSA SAF network was used as input. It has a 3.1 km spatial resolution (sub-satellite point) and daily frequency over the geostationary MSG grid (García-Haro et al., 2015). The MDFAPAR product is based on a linear relationship between the Renormalized Difference Vegetation Index (RDVI), computed from clear-sky top of the canopy reflectances in the red (R_R) and near infrared (R_{NIR}) bands for an optimal angular geometry in the solar principal plane (Roujean and Bréon, 1995). It was reported that the MSG f_{APAR} deviated from the other f_{APAR} products in the order of 0.1 (García-Haro et al., 2015).

In this study, the f_{APAR} time series were filtered and reconstructed using an optimized LOcally WEighted regression and Smoothing Scatterplots (LOWESS) method (Moreno et al., 2014; Gilabert et al., 2015), which captures the upper envelope of the time-series, interpolates the missing data and removes most of the noise of the original unfiltered signal. The LOESS approach is recommended in most remote sensing applications, such as gap-filling, cloud-replacement, and observing temporal dynamics *in situ* where rapid seasonal changes are produced (Moreno et al., 2014).

2.3. C_{ws}

The daily C_{ws} was computed using the daily AET LSA SAF product (DMET, LSA-302) and the daily PET derived from the JS parameterization (Eq. (4)). Eq. (4) uses the DIDSSF operational product delivered at the LSA SAF system and the daily mean T_a at SEVIRI/MSG disk (LSA SAF, 2016a). The T_a MSG product is derived from the interpolation of ERA-Interim data produced by the European Centre for Medium-Range Weather Forecasts (ECMWF, http://apps.ecmwf.int/datasets/), originally at 0.75° × 0.75°. The data are then interpolated to SEVIRI pixel scale by a bi-linearly interpolation method. The temperature fields are further adjusted to correct for the differences between ERA-Interim surface orography and pixel height, assuming a constant lapse rate of 0.67 °C/100 m. The interpolation procedure is designed to minimize the impact of model resolution.

DMET matches observed variations with a high compromise (*i.e.* product requirement criterion satisfied to a rate higher than 70% in most of the validation sites) for well-watered sites and an expected seasonal variation for temperate forests. It is also highly correlated with spatial variability in ECMWF daily-accumulated ET (correlation values from 0.85 to 0.95) (LSA SAF, 2010). However, the DMET product is underestimated globally in comparison with the ECMWF one, especially in Africa and South America (LSA SAF, 2010).

3. Data for MSG GPP assessment

The daily MSG GPP performance and assessment include: 1) qualitative evaluations of MSG GPP estimates in relation to characteristic spatial and seasonal patterns, 2) direct comparison of daily carbon flux estimates with *in situ* EC tower GPP estimations based on daily carbon flux measurements, and 3) consistency checking against other synergistic global carbon products. The data used for the proposed assessment are described below.

3.1. GPP estimates from eddy covariance flux towers

Daily GPP data from 18 EC flux towers were downloaded from the global Fluxes Database Cluster data set (FLUXNET). The FLUXNET2015 (http://fluxnet.fluxdata.org/) dataset consists of standardized and high quality data products collected from multiple regional EC flux networks (Valentini et al., 2014). The FLUXNET2015 GPP products were obtained applying standard flux-partitioning algorithms after the net ecosystem exchange time series were gap filled (Lasslop et al., 2010) and went through a rigorous QA/QC procedure (Pastorello et al., 2014). The model efficiency method reference GPP product (GPP_DT_VUT_REF) (Kumar et al., 2016) calculated using daily data (Lasslop et al., 2010) was compared with the MSG GPP estimates.

However, such direct comparison requires that the surface characteristics (vegetation composition) of the pixel used for RS products

Table 1
Description of EC sites located in Europe and Africa along with the main land cover percentage over a 5 km × 5 km GLC2000 window. The GLC2000 land cover of each site belongs to: CRO (croplands), DBF (deciduous broadleaf forest), EBF (evergreen broadleaf forest), ENF (evergreen needleleaf forest), MXF (mixed forest), SHR (shrublands), GRS (grasslands), or CRO (crops). PFT refers to the most representative plant functional type of the EC tower. SAV refer to savanna PFT.

Label	Name	Country	Latitude (°)	Longitude (°)	Altitude (m)	PFT	GLC2000	Main cover percentage (%)
CZ-BK1	Bily Kriz	Czech Republic	49,50	18,54	875	ENF	ENF	100
DE-SfN	Schechenfilz ord	Germany	47,81	11,33	590	ENF	ENF	80
FI-Let	Lettosuo	Finland	60,64	23,96	119	ENF	ENF	88
FI-Hyy	Hyytiala	Finland	61,85	24,29	181	ENF	ENF	80
FI-Sod	Sodankyla	Finland	67,36	26,64	180	ENF	ENF	92
IT-Lav	Lavarone	Italy	45,96	11,28	1353	ENF	ENF	44
DE-Hai	Hainich	Germany	51,08	10,45	430	DBF	CRO	72
DE-Lnf	Leinefelde	Germany	51,33	10,37	451	DBF	ENF	80
IT-Col	Collelongo	Italy	41,85	13,59	1560	DBF	DBF	96
DK-Sor	Soroe	Denmark	55,49	11,65	40	DBF	CRO	96
BE-Vie	Vielsalm	Belgium	50,31	5,99	493	DBF + ENF	ENF	92
FR-Pue	Puechabon	France	43,74	3,59	270	EBF	EBF	92
DE-Gri	Grillenburg	Germany	50,95	13,51	385	GRS	ENF	92
IT-MBo	Monte Bondone	Italy	46,01	11,05	1550	GRS	DBF	72
SN-Dhr	Dahra	Senegal	15,40	−15,43	40	GRS	CRO	100
Es-LMa	Las Majadas	Spain	39,94	−5,77	258	SAV	MXF	44
ZA-Kru	Skukuza	South Africa	−15,44	23,25	359	SAV	SHR	64
DE-Geb	Gebesee	Germany	51,10	10,91	161	CRO	CRO	100

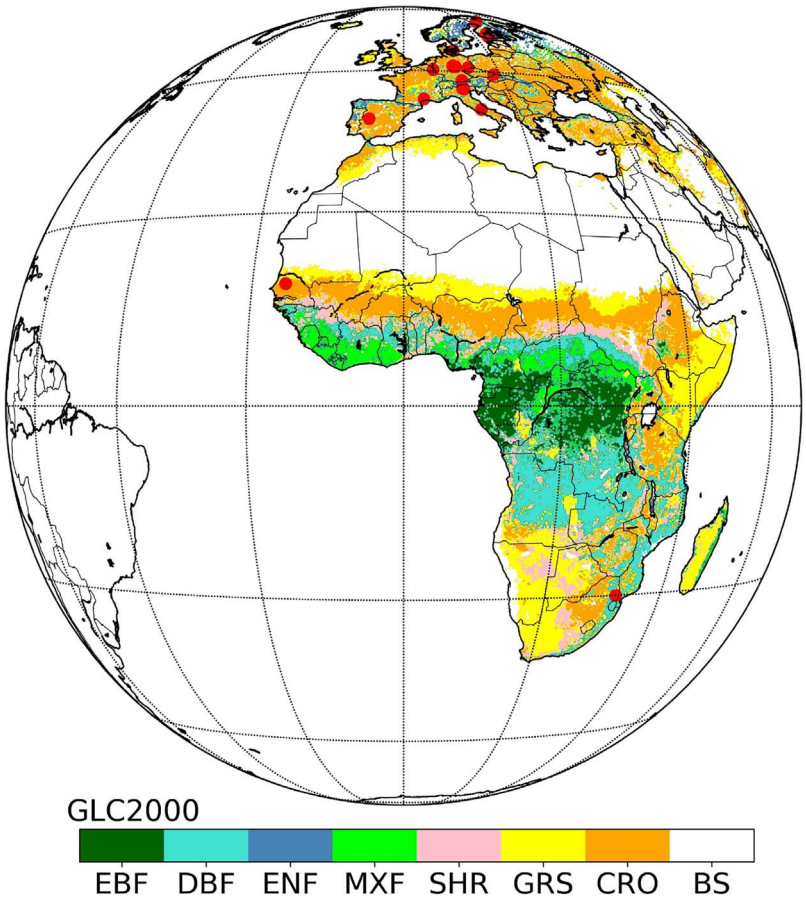

Fig. 1. The Global Land Cover 2000 (GLC2000) is shown. The GLC2000 has been geo-located and resampled to a standard SEVIRI grid. The selected EC sites are also included (red circles). A generalized thematic legend of 6 major land covers has been proposed in order to reduce the number of classes while preserving the essence of the geographical patterns of the study area. (For interpretation of the references to color in this figure legend, the reader is referred to the web version of this article.)

and of the EC measurements footprint are similar. To solve this issue, the homogeneity of a 5 km × 5 km area surrounding the measurement tower was analyzed. For this purpose, the 1 km Global Land Cover 2000 (GLC2000) (Bartholomé and Belward, 2005) was used. The selection of adequate sites for comparing MSG GPP and EC estimates without bias due to surface spatial heterogeneity was based on the following steps: 1) computation of the land cover percentages inside the 5i km × 5 km area (*i.e.* MSG pixel size over Europe) based on the GLC2000, 2) preselection of EC sites as those with two or less land cover classes within the 5ii km × 5 km area and one land cover percentage greater than 80%, and 3) final selection of EC sites by visual inspection using Google Earth™ (iiiTable 1). Fig. 1 shows the GLC2000 geo-located to a standard SEVIRI grid. The selected EC sites are also included (red crosses). A generalized classification was obtained by aggregating several similar land cover classes from the 23-class GLC2000. The study area was thus described through a generalized thematic legend of 6 major land covers: evergreen broadleaf forest (7%), deciduous broadleaf forest (13%), evergreen needleleaf forest (2%), mixed forest (5%), shrublands

(11%), grasslands (15%), croplands (15%) and bare soil (32%). This generalization reduces the number of classes while preserving the essence of the geographical patterns of the study area (Martínez et al., 2013).

3.2. MODIS GPP product (MOD17A2)

The MODIS GPP 8-day product (MOD17A2 version-55) at 1 km was retrieved from the online Reverb, courtesy of the NASA EOSDIS Land Processes Distributed Active Archive Center (LP DAAC), USGS/Earth Resources Observation and Science (EROS) Center, (https://reverb.echo.nasa.gov). Version-55 is post-processed from the MODIS GPP version-5 dataset, in which contaminated MODIS FPAR/LAI inputs to the MOD15 algorithm have been cleaned (Zhao and Running, 2010). The MODIS products were reprojected to Geographic (WGS84) coordinate projection and geo-located to a standard SEVIRI grid in order to reproduce the characteristics of the MSG product. The reprojection step was performed by averaging all fine resolution pixel values of the MODIS product that overlap with a given SEVIRI pixel. Pixels identified as water, snow or unreliable values were excluded during the averaging process (García-Haro et al., 2015).

3.3. FLUXCOM product

The FLUXCOM product provides monthly spatio-temporal fields at 0.5° × 0.5° spatial resolution for the period 1980–2013 from a combination of machine learning (ML) algorithms trained on site-level EC GPP estimates (www.fluxcom.org). The FLUXCOM data are available from the Data Portal of the Max Planck Institute for Biogeochemistry (www.bgc-jena.mpg.de/geodb/projects). The GPP fields are generated by 3 machine learning (ML) methods, namely, random forest (RF), artificial neural networks (ANN), and multivariate adaptive regression splines (MARS). The three methods are forced with meteorological data and mean seasonal cycles of several MODIS based variables (RS + METEO setup) on EC sites belonging to the FLUXNET La Thuile synthesis data set and CarboAfrica network (Valentini et al., 2014; Tramontana et al., 2016; Jung et al., 2017).

In this work, the GPP derived from the ANN (Papale and Valentini, 2003), which utilizes the relationship among the micrometeorological variables, was used. The application of ANN techniques to carbon flux dynamics study for European forest ecosystem has been demonstrated by several authors (*e.g.* Van Wijk and Bouten, 1999; Papale and Valentini, 2003). The FLUXCOM data were reprojected to Geographic (WGS84) coordinate projection at 1 km and the geo-located to a standard SEVIRI grid by the same procedure as for the MODIS data.

4. Results

4.1. Spatial and temporal MSG GPP patterns

Fig. 2 presents an overview of MSG GPP estimates showing one daily field every-two-months and covering a full year (2012). In general, maximum GPP values are observed in May-July in Europe and September-March in Africa (Fig. 2). The northern latitudes experience low GPP during winter and early spring due to prevalent cold temperatures and moderate radiation whereas GPP levels are high over the Equatorial belt throughout the whole year owing to relatively warm temperature, moist and radiation availability. GPP of semi-arid regions (*e.g.* South Spain, Sahel region, East Africa, South Africa) closely follows seasonality of rainy and dry seasons (Gilabert et al., 2015; Tagesson et al., 2016a; Räsänen et al., 2017). On the contrary, forest areas over Central Africa show the highest GPP estimates with values up to 8 g m^{-2} day^{-1}. This is one of the wettest parts of the continent with three common peak rainfall periods: March-April-May (MAM), July-August-September (JAS) and October-November-December (OND). There is a marked north–south split in Europe, with very wet conditions in Scandinavia and very dry conditions in much of central and south-east Europe. A reduction of GPP gaps due to cloud cover up to 72% is obtained when the daily f_{APAR} time series are filtered and reconstructed, located mainly in central Africa (10°S–10°N) and high latitudes (> 60°N).

4.2. Direct comparison with in situ EC tower GPP estimates

Fig. 3 shows the daily MSG GPP and the *in situ* EC GPP estimates from the FLUXNET EC towers (EC GPP). The MODIS and FLUXCOM GPP are also included for reference. The MSG GPP reproduces the seasonal variability in the EC GPP well, with low productivity values during winter and highest values during spring and summer. The MSG GPP time series show good performance to capture the GPP dynamics (r between 0.49 and 0.92) during the growing season, but less accurate in replicating GPP magnitude (rRMSE between 30% and 90%), which is mainly determined by ε_{max} (Fig. 2). At very high latitudes (*e.g.* North Europe), MSG GPP usually presents more gaps due to f_{APAR} missing values during winter. No MSG f_{APAR} values are calculated over areas covered by snow, by clouds during long periods, or with large uncertainties in the BRDF data (LSA SAF, 2016b).

The RS GPP products generally present a similar pattern (more detailed comparison is presented in Section 5). For ENF, one of the most productive vegetation types considered in the present study (*e.g.* EC sites in Finland, Italy and Germany), a mean biased error (MBE) lower than 40% is observed in most of the towers (Table 2) with a high agreement between MSG GPP and EC GPP values (r > 0.7). As might be expected, over ENF sites, MSG shows very low GPP in winter and peak GPP in summer. In these cases, the AET and PET show similar values (Fig. 4), confirming that such sites do not suffer water stress and main driving factors are radiation and temperature. A reduction of GPP gaps up to 56% is obtained for these sites when the daily f_{APAR} values are filtered (*e.g.* De-Sfn). The differences are assessed by means of the root mean square error (RMSE). The highest ENF EC towers disagreement is observed for FI-Let (RMSE = 3.9 g m^{-2} day^{-1}), and IT-Lav (RMSE = 3.4 g m^{-2} day^{-1}). A lower overall error and bias (RMSE = 2.76 g m^{-2} day^{-1} and MBE = −1.34 g m^{-2} day^{-1}) are obtained when considering all ENF sites (Fig. 5), observing a better agreement at EC GPP values lower than 7.0 g m^{-2} day^{-1} (distribution close to the 1:1 line).

For broadleaf flux towers, moderate (r = 0.69 for FR-Pue) to very good agreement (r = 0.92 for DE-Lnf) is observed between MSG GPP and EC GPP. The MSG GPP estimates agree with MODIS and FLUXCOM values, but the high EC GPP levels are not reached (*e.g.* DN-Lnf and Dk-Sor) giving an overall negative bias and RMSE = 3.62 g m^{-2} day^{-1} when all DBF towers are considered. For BE-Vie, DK-Sor, De-Lnf and DE-Hai discrepancies between the GLC2000 and the information provided by the tower (Table 1) are observed. These discrepancies are also present for the grassland (De-Gri, IT-MBo and SN-Dhr) and the savanna (ES-LMa, ZA-Kru) EC towers.

For grasslands towers IT-MBo and De-Gri, high correlations are observed (*e.g.* r up to 0.9 for IT-MBo). Although the main land cover type at both towers footprint is grassland, 72% of the land cover inside the 5 × 5 km area was determined as forest. The MSG GPP product is able to reproduce the seasonal behavior of this mixed forest (*i.e.* forest and grasslands) with large assimilation fluxes during the growing season (April-October) and to capture the GPP sharply decreased after the grass is mown in summer (*i.e.* DOY = 180 for IT-MBo and De-Gri and DOY = 210 for DE-Gri).

For the grassland (SN-Dhr) and savanna (ES-LMa) towers respectively in Senegal and Spain, the very high PET values when compared to AET (Fig. 4) indicate a high water demand during all year. Thus, accounting for water stress effect by means of the ratio AET/PET is a key feature of MSG GPP product at these sites. In the case of SN-Dhr, a low agreement of MSG GPP with the EC GPP estimates (and also MODIS and FLUXCOM) during the growing season is observed. The vegetation phenology

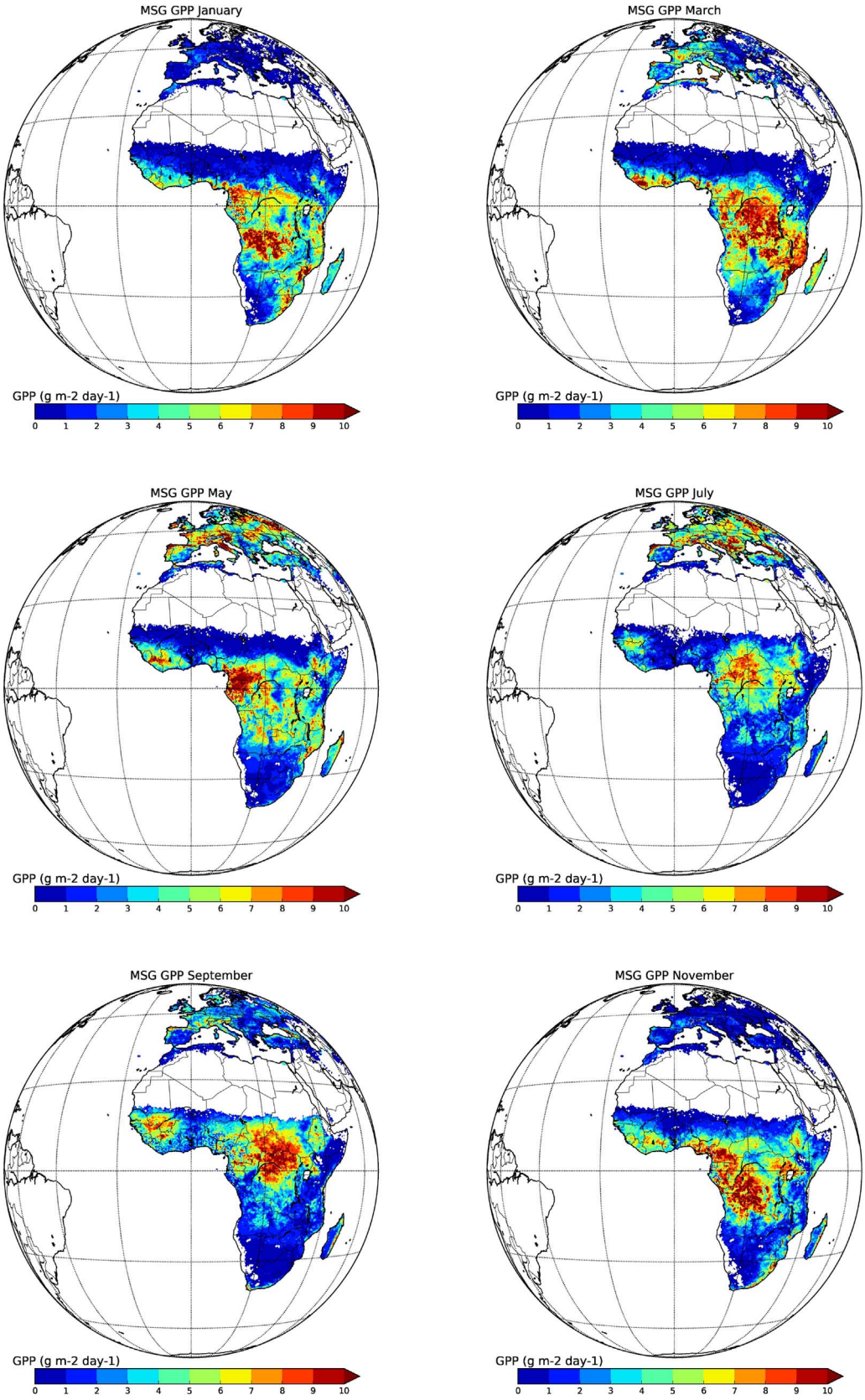

Fig. 2. Daily MSG GPP ($g\,m^{-2}\,day^{-1}$) images for a particular day every two months in 2012. The day chosen was as close to the middle of the month as possible.

maximum is generally not reached during solar solstice for semi-arid ecosystems since its seasonal variability is rather controlled by water availability (Tagesson et al., 2016a). In this case, the GPP is essentially driven by f_{APAR} as also suggested when the seasonal patterns of GPP and f_{APAR} (Fig. 4) are compared. For grasslands and savanna, a higher agreement (RMSE = 2.11 $g\,m^{-2}\,day^{-1}$; MBE = −0.63 $g\,m^{-2}\,day^{-1}$) is observed between the MSG GPP and EC GPP estimates with a 60% of the EC GPP variance explained by the MSG GPP (Fig. 5d).

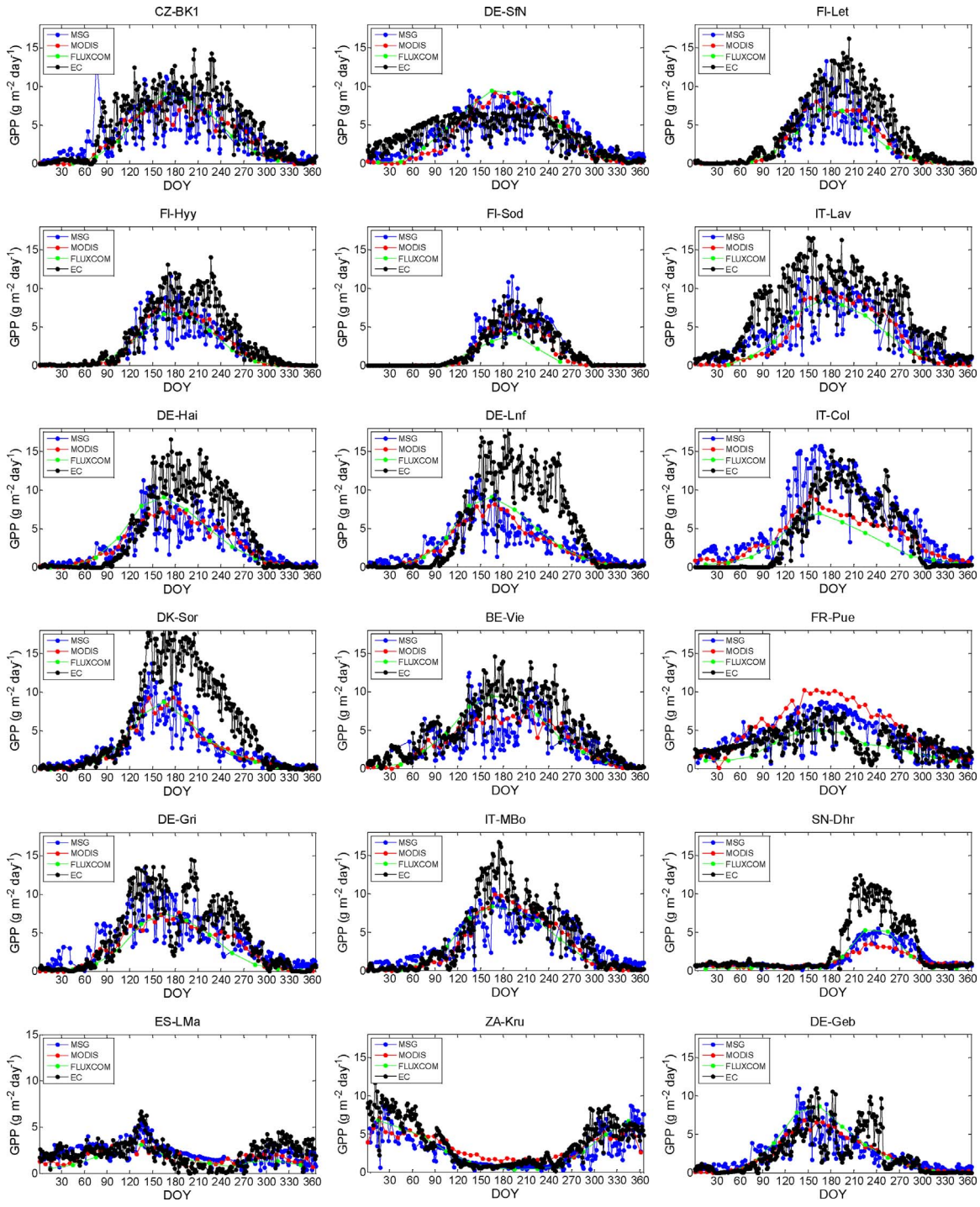

Fig. 3. Temporal profiles of daily MSG GPP, 8-day MODIS GPP and monthly FLUXCOM GPP together with EC GPP data at de different FLUXNET EC towers.

4.3. Consistency checking with synergistic global satellite carbon products

The MSG GPP provides similar or lower errors than MODIS and FLUXCOM at seven of the twelve forest towers when compared with *in situ* EC GPP (Table 1; CZ-BK1, FI-Sod, IT-Lav, De-Hai, IT-Col, Be-Vie and FR-Pue), as well as at ES-LMa and SN-Dhr sites (Table 3). In general, an underestimation is observed for the three RS products, being larger at the most productive DBF and ENF sites, such as DK-Sor, DE-Hai, DE-Lnf and FI-Let.

An overestimation is observed at two broadleaf forest towers (IT-Col and FR-Pue) and at DE-SfN during the growing season. At DE-SfN, the three RS products show higher values than EC GPP whereas FLUXCOM provides lower values at IT-Col and FR-Pue. At FR-Pue, the MODIS and FLUXCOM products show, respectively, the highest and lowest GPP estimates, whereas MSG GPP provides intermediate GPP values, more in agreement with the EC flux tower (*i.e.* MBE = 0.7 g m^{-2} day^{-1}, RMSE = 1.8 g m^{-2} day^{-1} at 8-day temporal resolution). A higher constant MODIS f_{APAR} value (~0.7 at https://modis.ornl.gov/fixedsite/) than MSG f_{APAR} during all year along with the maximum value of radiation at the growing season could explain the higher GPP levels obtained for MODIS GPP. The highest discrepancy between the three RS products and EC GPP are observed for DK-Sor, DE-Hai, and FI-Let sites.

In general, a good agreement is observed between the MSG GPP and EC GPP estimates when the MSG GPP is re-sampled to 8-day and

Table 2
Statistics of the MSG GPP direct comparison between MSG GPP and GPP EC. The mean bias error (MBE), mean absolute error (MAE) and root mean square error (RMSE) are given in $g\,m^{-2}\,day^{-1}$, and their relative values (rMBE, rMAE and rRMSE) in %. The correlation coefficient (r) is also shown.

SITE FLUXNET ID	MBE (rMBE)	MAE (rMAE)	RMSE (rRMSE)	r
CZ-BK1	−1.3 (−29)	1.7 (36)	2.3 (50)	0.91
DE-SfN	−0.1 (−2)	1.1 (33)	1.4 (42)	0.85
FI-Let	−3.2 (−38)	3.3 (39)	3.9 (47)	0.71
FI-Hyy	−2.3 (−32)	2.5 (35)	3.1 (42)	0.72
FI-Sod	0.2 (4)	1.0 (17)	1.3 (25)	0.74
IT-Lav	−2.4 (−39)	2.5 (39)	3.4 (54)	0.88
DE-Hai	−1.6 (−35)	2.3 (52)	3.3 (75)	0.87
DE-Lnf	−2.2 (−45)	3.2 (65)	4.6 (94)	0.77
IT-Col	1.5 (36)	1.9 (46)	2.4 (57)	0.92
DK-Sor	−2.9 (−51)	3.2 (56)	4.7 (83)	0.88
BE-Vie	−2.1 (−35)	2.3 (38)	3.0 (50)	0.81
FR-Pue	0.7 (23)	1.4 (43)	1.9 (60)	0.69
DE-Gri	−0.6 (−13)	1.7 (40)	2.4 (56)	0.84
IT-MBo	−0.6 (−13)	1.6 (38)	2.3 (56)	0.90
SN-Dhr	−1.0 (−41)	1.3 (51)	2.3 (92)	0.89
ES-LMa	−0.1 (−4)	1.0 (49)	1.2 (58)	0.49
ZA-Kru	−1.1 (−28)	1.5 (37)	2.1 (52)	0.78
DE-Geb	−0.1 (−3)	1.3 (55)	1.8 (80)	0.73

Note: Correlations were statistically significant at 95% confidence level.

monthly temporal resolution (Fig. 6a and b). The computed statistics are in agreement with those derived for the MODIS product. A MBE lower than $1.5\,g\,m^{-2}\,day^{-1}$ is obtained for all the canopies. Although the higher RMSE is still observed for the DBF land cover, it is still lower than MODIS outcomes. At monthly temporal resolution, the MSG GPP errors decrease when considering all the EC towers except those corresponding to DBF (MBE $< -1.08\ g\,m^{-2}\,day^{-1}$), being lower than those observed for the FLUXCOM product.

The differences between MSG with MODIS and FLUXCOM are spatially assessed by means of the annual root mean square difference (RMSD) and mean bias difference (MBD) (Fig. 7). For Europe, the differences between the three RS products are very low. The differences are slightly lower when the MSG and MODIS are compared, particularly over South Europe and North and South Africa. The major GPP disagreement arises over moist biomes (*e.g.* tropical forests in central Africa) with RMSD values up to $3.0\,g\,m^{-2}\,day^{-1}$ and over dry biomes (*e.g.* semi-arid, savanna and transitional woodlands) with MSG GPP estimates lower than FLUXCOM (*e.g.* MBD values up to $-3.0\,g\,m^{-2}\,day^{-1}$). Particularly, MODIS and FLUXCOM provide larger differences for the humid savanna ecosystems of west and central Africa (MBD values up to $2.0\,g\,m^{-2}\,day^{-1}$).

The annual spatial patterns for MSG, MODIS, and FLUXCOM GPP (Fig. 8) are compared. The three estimates agree reasonably well, although differences are significant in some areas. Specifically, there is a good agreement in Europe and North and South Africa, but MSG GPP is lower than FLUXCOM and MODIS over central Africa. The largest differences occur in Equatorial areas covered by tropical forest where MODIS and FLUXCOM estimates are around $3500\,g\,m^{-2}\,yr^{-1}$, while annual MSG GPP is below $3000\,g\,m^{-2}\,yr^{-1}$.

5. Discussion

The retrieval of MSG GPP estimates from an optimized Monteith's model is presented. The MSG GPP product reproduces the EC GPP and its seasonal variability over most ecosystems. MBE values lower than 40% in most of the towers are found for the most efficient forest vegetation types. These MSG GPP values lie within the total uncertainty range for EC GPP proposed by Schaefer et al. (2012) as well as those obtained with coarse spatial resolution derived products (*e.g.* the Soil Moisture Active Passive global GPP product at 9 km (Kimball et al., 2016)). For the MODIS GPP product, average errors of 50% for non-forested ecosystems and larger underestimation (61%) for croplands were reported by Yang et al. (2007). The current MOD17A2 product is highly effective for MF (mixed forests) and DBF, moderately effective for ENF, and ineffective for EBF (Tang et al., 2015). Several factors have been discussed among possible causes for such differences that could also explain MSG GPP disagreements. These include diffusion radiation (Jenkins et al., 2007), f_{APAR} estimates (Zhao et al., 2011), the maximum light use efficiency (Yang et al., 2007), or differences in spatiotemporal coverage (Heinsch et al., 2006; Yang et al., 2007).

Particularly, the MSG GPP product shows a high ability to cope with water stress during the dry season at sites in Senegal and Spain (SN-Dhr and ES-LMa). Both sites are a typical low tree and shrub savanna

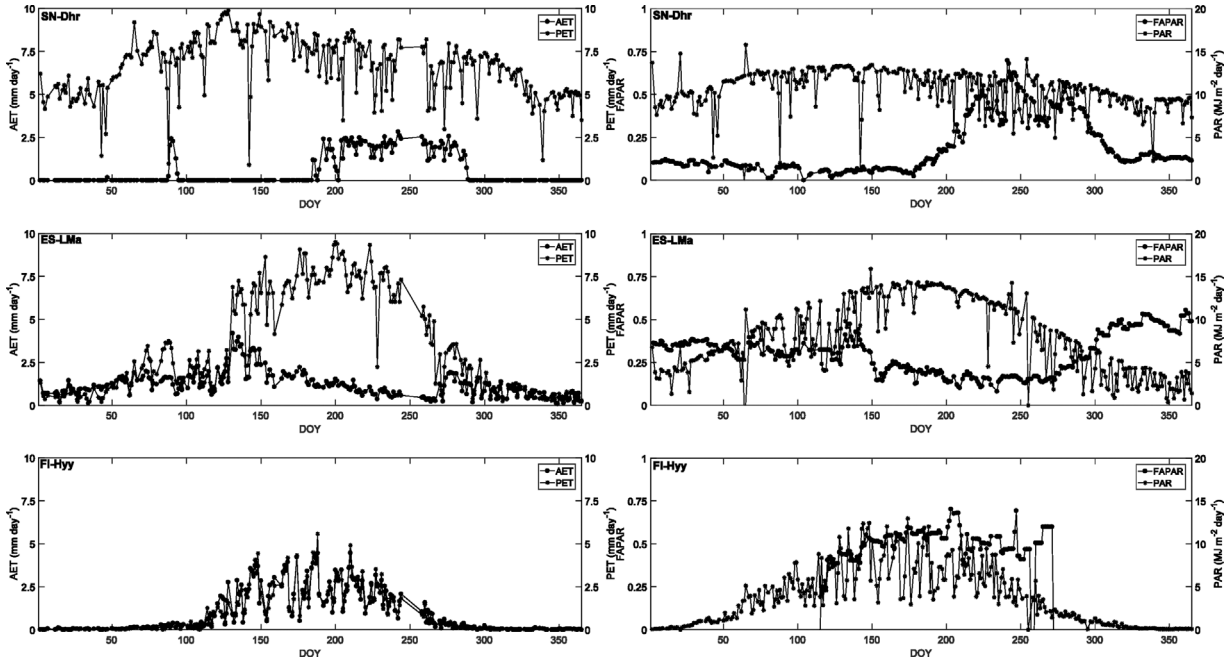

Fig. 4. Temporal variation of AET and PET (left) as well as f_{APAR} and PAR (right) for two sites with water shortage limitations, SN-Dhr (Senegal) and ES-LMa (Spain), and a non-water limited typical forest ecosystem site in Finland, FI-Hyy, for 2012.

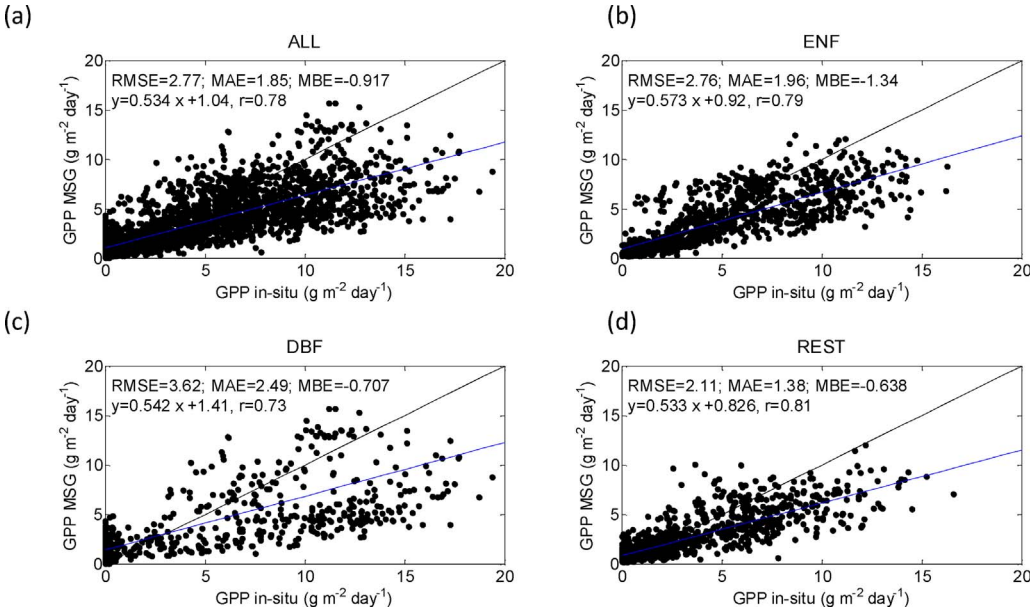

Fig. 5. Evaluation of the MSG GPP against *in situ* EC GPP for the all the sites (a) and for the sites according to ENF (b), DBF (c) and rest of land covers (d). The black lines show the one-to-one ratios, whereas the blue lines are the fitted ordinary least square regression. (For interpretation of the references to color in this figure legend, the reader is referred to the web version of this article.)

Table 3
Statistics resulting from the comparison of the three RS GPP products with the *in situ* EC GPP estimates. The MBE, MAE and RMSE are in g m^{-2} day^{-1}. The daily MSG GPP was resampled to the temporal resolution of MODIS (8 days) and FLUXCOM (1 month). The correlation coefficients (*r*) are presented.

		MBE	RMSE	r		MBE	RMSE	*r*
CZ-BK1	MSG_{8days}	−1.5	2.2	0.97	$MSG_{monthly}$	−1.3	1.9	0.99
	MODIS	−1.5	2.0	0.95	FLUXCOM	−1.8	2.3	0.89
DE-SfN	MSG_{8days}	−0.1	1.0	0.91	$MSG_{monthly}$	−0.2	1.0	0.88
	MODIS	−0.01	1.8	0.85	FLUXCOM	0.3	2.2	0.83
FI-Let	MSG_{8days}	−3.1	3.6	0.81	$MSG_{monthly}$	−2.6	3.1	0.85
	MODIS	−2.7	3.1	0.88	FLUXCOM	−2.9	3.2	0.92
FI-Hyy	MSG_{8days}	−2.3	2.8	0.74	$MSG_{monthly}$	−1.8	2.4	0.78
	MODIS	−1.9	2.3	0.87	FLUXCOM	−1.9	2.2	0.88
FI-Sod	MSG_{8days}	−0.12	0.7	0.88	$MSG_{monthly}$	0.1	0.3	0.98
	MODIS	−0.4	0.9	0.85	FLUXCOM	−2.0	2.1	0.88
IT-Lav	MSG_{8days}	−2.3	3.2	0.90	$MSG_{monthly}$	−2.8	3.4	0.92
	MODIS	−2.7	3.5	0.87	FLUXCOM	−4.2	4.4	0.89
DE-Hai	MSG_{8days}	−1.6	3.2	0.91	$MSG_{monthly}$	−1.4	2.9	0.91
	MODIS	−1.5	3.0	0.91	FLUXCOM	−1.1	2.9	0.78
DE-Lnf	MSG_{8days}	−2.2	4.6	0.81	$MSG_{monthly}$	−1.9	4.2	0.76
	MODIS	−2.3	4.2	0.88	FLUXCOM	−1.6	3.3	0.83
IT-Col	MSG_{8days}	1.4	2.0	0.95	$MSG_{monthly}$	1.7	2.1	0.95
	MODIS	−0.4	2.5	0.92	FLUXCOM	−1.4	3.1	0.83
DK-Sor	MSG_{8days}	−2.8	4.6	0.90	$MSG_{monthly}$	−2.7	4.3	0.91
	MODIS	−2.9	4.4	0.93	FLUXCOM	−2.8	4.2	0.92
BE-Vie	MSG_{8days}	−2.1	2.7	0.88	$MSG_{monthly}$	−1.9	2.6	0.87
	MODIS	−2.1	2.6	0.92	FLUXCOM	−1.2	2.0	0.88
FR-Pue	MSG_{8days}	0.7	1.8	0.64	$MSG_{monthly}$	0.7	1.5	0.78
	MODIS	2.0	3.2	0.67	FLUXCOM	−0.7	1.1	0.82
DE-Gri	MSG_{8days}	−0.7	2.3	0.88	$MSG_{monthly}$	−0.5	1.7	0.94
	GPP MODIS	−1.4	2.5	0.90	FLUXCOM	−1.8	2.4	0.92
IT-MBo	MSG_{8days}	−0.4	1.9	0.93	$MSG_{monthly}$	−0.6	2.1	0.96
	MODIS	−0.6	1.2	0.96	FLUXCOM	−1.0	2.0	0.91
SN-Dhr	MSG_{8days}	−1.0	2.2	0.90	$MSG_{monthly}$	−1.1	2.1	0.94
	MODIS	−1.3	2.6	0.90	FLUXCOM	−1.2	1.9	0.93
ES-LMa	MSG_{8days}	−0.2	1.0	0.60	$MSG_{monthly}$	0.02	0.8	0.63
	MODIS	−0.6	1.6	0.90	FLUXCOM	−0.6	1.1	0.57
ZA-Kru	MSG_{8days}	−1.1	1.7	0.90	$MSG_{monthly}$	−1.1	1.5	0.96
	MODIS	−0.7	1.6	0.80	FLUXCOM	−0.8	1.2	0.94
DE-Geb	MSG_{8days}	−0.2	1.6	0.80	$MSG_{monthly}$	0.1	1.3	0.80
	MODIS	−0.2	1.4	0.84	FLUXCOM	0.7	1.9	0.81

Note: Correlations were statistically significant at 95% confidence level.

environment with a low tree cover (Tagesson et al., 2015; Sánchez-Ruiz et al., 2017). However, larger discrepancies with EC GPP are found during the growing season, especially at SN-Dhr. Tagesson et al. (2017) explained the strong underestimation of the MODIS GPP product for the Sahel arguing that the ε_{max} is set too low (~0.85 g MJ^{-1}) in relation to *in situ* based estimates (1.58–3.50 g MJ^{-1}). Additionally, the EC GPP in SN-Dhr is high in relation to other semi-arid ecosystems; these high values have been explained, among others, by relatively dense ground vegetation and high soil nutrient availability (Tagesson et al., 2016a; Tagesson et al., 2016b). These parameters are not included in the satellite-based models possibly explaining these discrepancies. However, the low RMSE obtained in SN-Dhr and ES-LMa still indicate the strong applicability of the AET/PET ratio as a limiting factor in the Monteith model for drylands.

Furthermore, main uncertainties may be associated to scale mismatches between the EC footprint and the RS data. This could explain the highest disagreement observed for some of ENF (*e.g.* FI-Let, DE-SfN and IT-Lav) between the EC GPP and the GPP derived from the RS products. At DE-SfN, the canopy belongs to a natural peatland forest dominated by slow growing bog-pines and ground layer vegetation dominated by peat mosses (Hommeltenberg et al., 2014). As pine dominates the vegetation in the footprint area of the EC tower, the early rise of GPP (EC GPP and MSG GPP) in the year is likely due to the early start of photosynthesis of pine. During the course of the year, the overestimation of GPP in summer by the MSG GPP approach may also be a result of the pine dominated GPP which is lower compared to the classical peatbog vegetation. Although the overestimation is observed for the RS products, the early rise of EC GPP is only captured by the MSG GPP product. At IT-Lav, the forest is dominated by coniferous trees, but the EC site representativeness showed 32% cover by mixed forest and 8% by DBF, which explains the GPP lower values for MSG GPP and the temporal delay that the RS GPP products show at the beginning of the growing season. The FI-Let tower is a very homogeneous site compound by a mixture of scots pine and pubescent birch in the dominant canopy layer (Korkiakoski et al., 2017). In this site, the favorable water conditions (AET and PET ratio close to one) along with expected f_{APAR} and PAR values lead to think in other limiting factors that may affect the GPP predictions. 1) The SEVIRI/MSG observation geometry causes large uncertainties, mainly in wintertime, as a combination of multiple effects, such as low illumination angles, higher anisotropy, higher cloud occurrence, larger shadows or traces of snow cover. 2) GPP of forest ecosystems at high latitudes (> 60°N) is greatly limited by low air temperature, a short growing season, and radiation availability (Anav et al., 2015).

The mismatch between the EC footprint and the MSG pixel size can

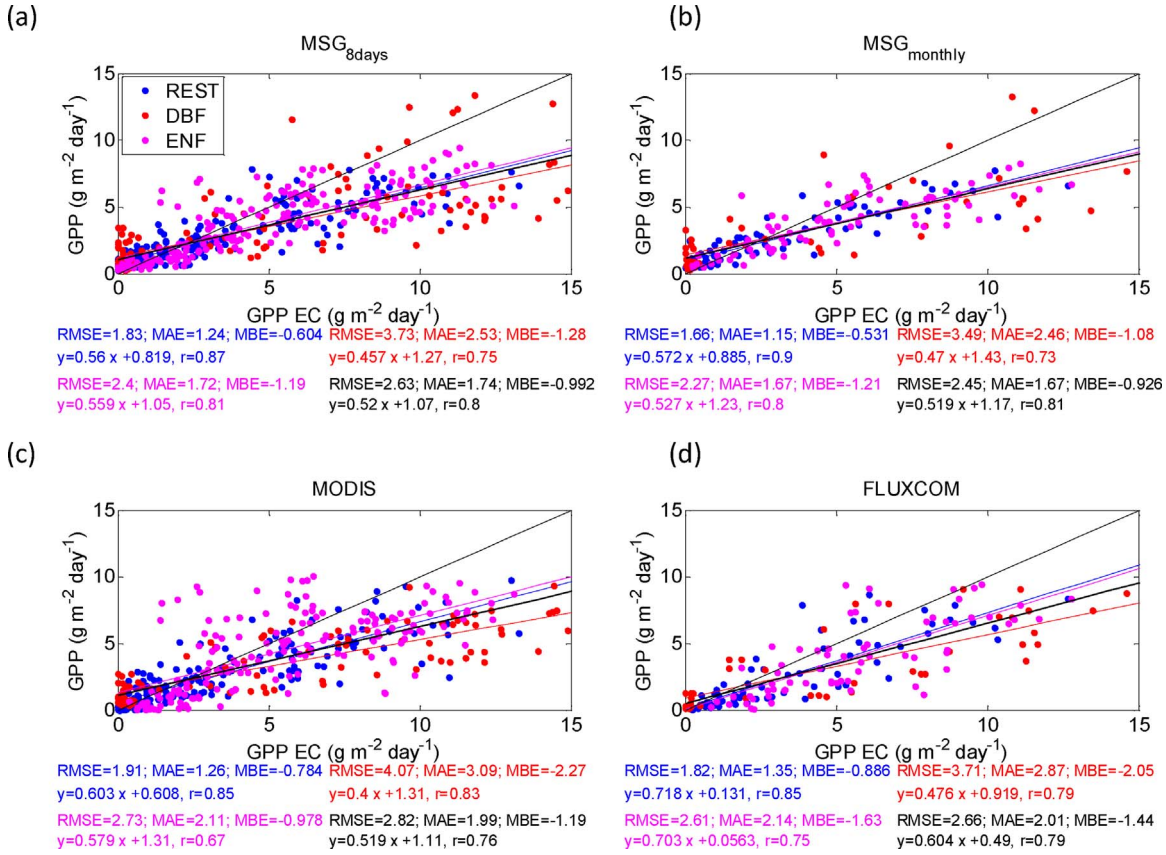

Fig. 6. MSG GPP re-sampled at 8-day (a) and monthly (b) temporal resolutions against EC GPP values. MSG along with GPP MODIS (c) and GPP FLUXCOM (d) *vs*. EC GPP are also presented. The RMSE, MAE, MBE, *r* and linear regression are computed for the ENF (magenta), DBF (red), REST (blue) and ALL (black) sites. The black thin lines show the one-to-one ratios. The thick black lines show the fitted ordinary least square regression when all sites are considering. The red, magenta and blue lines show the fitted ordinary least square regression for the DBF, ENF and REST flux towers. (For interpretation of the references to colour in this figure legend, the reader is referred to the web version of this article.)

also explain the diminution of GPP on DBF towers at the end of the summer (DE-Hai, DE-Lnf, DK-Sor). However, the MSG GPP discrepancies found for DBF at Denmark and Germany (*e.g.* DK-Sor, DE-Hai and DE-Lnf) could be reduced if the ε_{max} would be better adjusted. At DK-Sor and DE-Hai, a crop $\varepsilon_{max} = 1.2\ g\ MJ^{-1}$ was set instead of a deciduous broadleaf forest $\varepsilon_{max} = 1.8\ g\ MJ^{-1}$, substantially lowering MSG GPP. A reduction of rMBE respectively to 31% and 6% could be achieved if ε_{max} would be adjusted accordingly. Quaife et al. (2008) estimated that the error in GPP introduced from satellite derived land cover is up to 16%. An overall accuracy of 68.6% was reported for GLC2000 at a global scale (Mayaux et al., 2006). Thus, the wrong assignment of GLC2000 classes has a negative impact on MSG GPP values where a more accurate land cover map would thereby improve the performance of the MSG GPP product.

Another important factor that limits photosynthesis is cloud cover. Although the reduction of carbon uptake by photosynthesis due to cloud cover is primarily assumed by the diminution of the radiation input, the GPP estimates could be limited by the reliability of biophysical parameters such as f_{APAR} and leaf area index due to the lack of an operational and efficient cloud filtering. The filter and reconstruction of the MSG f_{APAR} time series allowed reducing the overall error of the GPP estimates. When the three RS products are intercompared, the observations used for the comparison may differ due to the availability and nominal temporal sampling interval, which could be hampered by missing data mainly due to cloud occurrence. In case of MSG GPP, the daily basis will allow performing gap filling and filtering techniques for an accurate depiction of vegetation dynamics and correct the diminution of GPP due to spectral cloud contamination, as it takes place on tropical forests.

At regional level, the MSG GPP estimates are similar to MODIS and FLUXCOM ones over the temperate zones whereas the largest discrepancies are observed over the tropical zone. In the tropics, large differences are also detected between MODIS and FLUXCOM. A poor relatively FLUXCOM GPP prediction was expected in the tropics due to an undersampled training data (Tramontana et al., 2016). Differences could also be attributed to GPP low quality due to contamination from cloudiness (*i.e.* affecting MSG and MODIS f_{APAR} products) and poor constraints on meteorological reanalysis datasets affecting MODIS GPP product (Zhao et al., 2006). Moreover, the underestimation of MSG GPP values for the tropical region may be explained by, i) systematic low MSG f_{APAR} values reported over needleleaf and broadleaf forests (Martínez et al., 2013) and ii) uncertainties introduced by an overestimation of PET derived from the JS approach over broadleaf forest (Vörösmarty et al., 1998). This pattern is consistent with the finding by Zhao et al. (2006), which showed that the tropical region has the largest uncertainties in MODIS GPP.

The selection of only one year was justified by a trade-off between the availability of necessary input data for the other years from LSA-SAF and the major representativeness of EC GPP data for validation purposes. To evaluate the reliability and performance of the method for daily MSG GPP retrievals it was required to capture and monitor the GPP magnitude and seasonal variability for at least one year. However, a longer GPP time-series consisting of inter-annual variability would improve the model evaluation and this is possible as the data availability from LSA-SAF increases. Additionally, as new MSG products appear in the LSA SAF system, these can be incorporated in the C_{ws} parameterization to improve the model accuracy, such as the daily reference evapotranspiration (DMETREF, LSA-303).

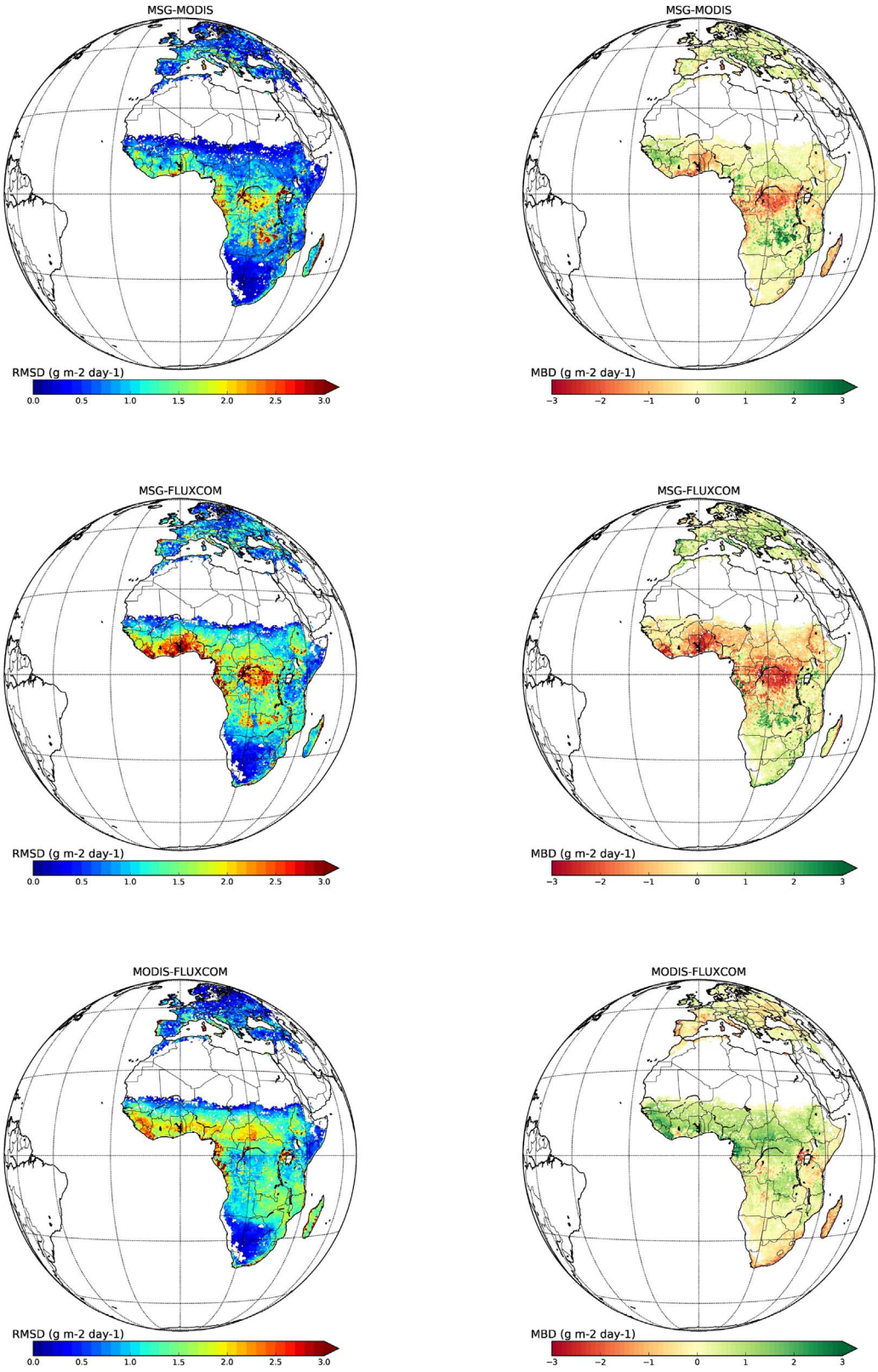

Fig. 7. Annual root mean square difference (RMSD) and mean bias difference (MBD) (in g m^{-2} day^{-1}) between MSG-MODIS (top), MSG-FLUXCOM (centre) and MODIS-FLUXCOM (bottom.)

6. Summary and conclusions

This study aimed to provide a method for daily GPP estimates over Europe and Africa based on an ensemble of SEVIRI/MSG available products. The proposed framework takes advantage of the LSA SAF system facilities, and uses operational SEVIRI/MSG products to measure the absorbed photosynthetic active radiation (APAR) by vegetation (*i.e.* the product by PAR and f_{APAR}) and the environmental variables that affect the use of this absorbed flux in primary production (Trigo et al., 2011). This newly derived product has the potential for analyzing spatial patterns and temporal dynamics of GPP at the MSG spatial resolutions on a daily basis. The real challenge was to capture

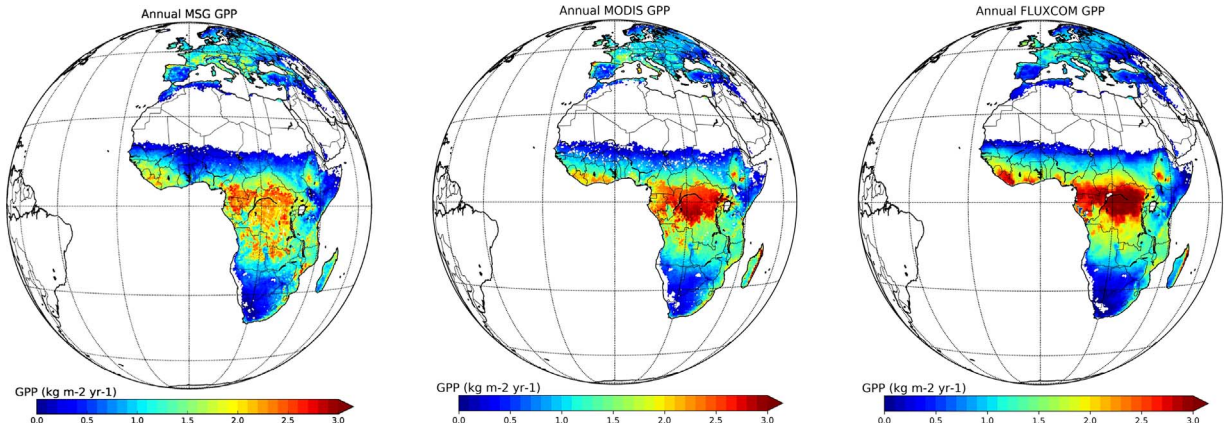

Fig. 8. Annual GPP estimates for MSG, MODIS and FLUXCOM.

GPP dynamics and magnitude during the growing season. We would like to highlight the MSG GPP performance in relation to three aspects:

1) The ability to capture the intra-annual variability of carbon cycle. The new MSG GPP product has a daily temporal resolution, which is a major advantage in relation to previous satellite based GPP products in the study of intra-annual dynamics of GPP.
2) The capability to identify possible reduction of productivity due to water shortage which is very important in dry-lands. The MSG GPP estimates introduce the advantage of considering the C_{ws} water stress factor by means of a global AET product generated also with MSG data as well as a parameterized potential ET by means of air temperature.
3) The potential to provide a new GPP product with at least equally high confidence as compared to other satellite derived GPP products. An evaluation against independent *in situ* data indicated that the uncertainties of the daily MSG GPP estimates are similar to those shown by other satellite products, such as MODIS and FLUXCOM.

This study broadens the applicability of SEVIRI/MSG products for deriving reliable carbon uptake estimates over Europe and Africa. The coarser spatial resolution of SEVIRI is compensated by the availability of combining different MSG products at daily temporal coverage that can contribute to increased knowledge regarding changes in GPP (*e.g.* daily, seasonally or yearly) as well as higher precision in GPP accumulated values.

Acknowledgements

This research was supported by the LSA SAF (EUMETSAT) and ESCENARIOS project from the Spanish Ministry of Economy and Competitiveness (CGL2016-75239-R). This work used eddy covariance data acquired and shared by the FLUXNET community. The FLUXNET eddy covariance data processing and harmonization was carried out by the European Fluxes Database Cluster, AmeriFlux Management Project, and Fluxdata project of FLUXNET, with the support of CDIAC and ICOS Ecosystem Thematic Center, and the OzFlux, ChinaFlux and AsiaFlux offices. The ERA-Interim reanalysis data were provided by ECMWF and processed by LSCE. We also thank M. Jung for providing FLUXCOM GPP. The funding of SNSB (Dnr 95/16) for T. Tagesson and the Helmholtz Association and the Federal Ministry of Education and Research (BMBF) in the framework of TERENO (Terrestrial Environmental Observatories) and ICOS (Integrated Carbon Observation System) are also acknowledged.

Appendix A. Supplementary data

Supplementary data associated with this article can be found, in the online version, at http://dx.doi.org/10.1016/j.jag.2017.10.011.

References

Anav, A., et al., 2015. Spatiotemporal patterns of terrestrial gross primary production: a review. Rev. Geophys. 53, 785–818. http://dx.doi.org/10.1002/2015RG000483.
Bartholomé, E., Belward, A.S., 2005. GLC2000: a new approach to global land cover mapping from Earth observation data. Int. J. Remote Sens. 26 (9), 1959–1977.
EEA, 2012. Climate change, impacts and vulnerability in Europe 2012. An indicator-based report. EEA Report No 12/2012. European Environment Agency, Copenhagen, Denmark.
Fisher, J.B., Whittaker, R.J., Malhi, Y., 2011. ET come home: potential evapotranspiration in geographical ecology. Global Ecol. Biogeogr. 20, 1–18.
Garbulsky, M.F., et al., 2010. Patterns and controls of the variability of radiation use efficiency and primary productivity across terrestrial ecosystems. Glob. Ecol. Biogeogr. 19, 253–267.
García-Haro, F.J., Camacho, F., Martínez, B., Meliá, J., 2015. Validation Report Vegetation Parameters (VEGA), SAF/LAND/UV/VR_VEGA/2.0. Available on-line at. http://landsaf.meteo.pt.
Geiger, B., Meurey, C., Lajas, D., Franchistéguy, L., Carrer, D., Roujean, J.-L., 2008. Near real time provision of downwelling shortwave radiation estimates derived from satellite observations. Meteorol. Appl. 15, 411–420.
Gilabert, M.A., et al., 2015. Daily GPP estimates in Mediterranean ecosystems by combining remote sensing and meteorological data. ISPRS J. Photogramm. Remote Sens. 102, 184–197.
Heinsch, F.A., et al., 2006. Evaluation of remote sensing based terrestrial productivity from MODIS using regional tower eddy flux network observations. IEEE Trans. Geosci. Remote Sens. 44 (7), 1908–1925.
Hommeltenberg, J., Schmid, H.P., Drösler, M., Werle, P., 2014. Can a bog drained for forestry be a stronger carbon sink than a natural bog forest? Biogeosciences 11, 3477–3493.
IPCC, 2014. Climate Change 2014: Impacts, Adaptation, and Vulnerability. Cambridge University Press, Cambridge, United Kingdom and New York, NY, USA.
Idso, S.B., Jackson, R.D., Pinter, P.J., Reginato, R.J., Hatfield, J.L., 1981. Normalizing the stress-degree-day parameter for environmental variability. Agric. For. Meteorol. 24, 45–55.
Iqbal, M., 1983. An Introduction to Solar Radiation. Academic Press, Toronto 390 pp.
Jenkins, J.P., Richardson, A.D., Braswell, B.H., Ollinger, S.V., Hollinger, D.Y., Smith, M.-L., 2007. Refining light-use efficiency calculations for a deciduous forest canopy using simultaneous tower-based carbon flux and radiometric measurements. Agric. For. Meteorol. 143, 64–79.
Jensen, M.E., Haise, H.R., 1963. Estimating evapotranspiration from solar radiation. J. Irrig. Drain. Div. 89, 15–41.
Jung, M., et al., 2017. Compensatory water effects link yearly global land CO2 sink changes to temperature. Nature 541. http://dx.doi.org/10.1038/nature20780.
Kimball, J.S., Jones, L.A., Glassy, J., Stavros, E.N., Madani, N., Reichle, R.H., Jackson, T., Colliander, A., 2016. Soil Moisture Active Passive (SMAP) Mission Assessment Report for the Version 2 Validated Release L4_C Data Product. GMAO Office Note No. 13 (Version 1.0). NASA Goddard Space Flight Center, Greenbelt, MD, USA 37 pp.
Korkiakoski, M., et al., 2017. Methane exchange at the peatland forest floor – automatic chamber system exposes the dynamics of small fluxes. Biogeosciences 14, 1947–1967. http://dx.doi.org/10.5194/bg-14-1947-2017.
Kumar, J., Hoffman, F.M., Hargrove, W.W., Collier, N., 2016. Understanding the representativeness of FLUXNET for upscaling carbon flux from eddy covariance measurements. Earth Syst. Sci. Data Discuss. 1–25. http://dx.doi.org/10.5194/essd-2016-36.
LSA SAF, 2010. Algorithm Theoretical Basis Document (ATBD) for MSG Evapotranspiration (MET) and Daily MET (DMET) Product. SAF/LAND/IM/ATBD_MET/1.2. Available on-line at. http://landsaf.meteo.pt.
LSA SAF, 2012. Algorithm Theoretical Basis Document (ATBD) for Down-Welling Surface Shortwave Flux (DSSF). SAF/LAND/MF/ATBD_DSSF/1.0. Available on-line at.

http://landsaf.meteo.pt.
LSA SAF, 2016a. Algorithm Theoretical Basis Document (ATBD) for Reference Evapotranspiration (DMETREF). SAF/LAND/IPMA/ATBD_METREF/1.0. Available on-line at. http://landsaf.meteo.pt.
LSA SAF, 2016b. Algorithm Theoretical Basis Document for Vegetation Parameters (VEGA). PRODUCTS: LSA-421 (MDFVC), LSA-422 (MTFVC), LSA-423 (MDLAI), LSA-424 (MTLAI), LSA-425 (MDFAPAR), LSA-426 (MTFAPAR), LSA-450 (MTFVCR), LSA-451 (MTLAI-R), LSA-452 (MTFAPAR-R). SAF/LAND/UV/VR_VEGA/2.0. Available on-line at. http://landsaf.meteo.pt.
Lasslop, G., et al., 2010. Separation of net ecosystem exchange into assimilation and respiration using a light response curve approach: critical issues and global evaluation. Glob. Change Biol. 16, 187–208. http://dx.doi.org/10.1111/j.1365-2486.2009.02041.x.
Martínez, B., Camacho, F., Verger, A., García-Haro, F.J., Gilabert, M.A., 2013. Intercomparison and quality assessment of MERIS: MODIS and SEVIRI FAPAR products over the Iberian Peninsula. Int. J. Appl. Earth Obs. Geoinf. 21, 463–476.
Maselli, F., Papale, D., Puletti, N., Chirici, G., Corona, P., 2009. Combining remote sensing and ancillary data to monitor the gross productivity of water-limited forest ecosystems. Remote Sens. Environ. 113, 657–667.
Maselli, F., Argenti, G., Chiesi, M., Angeli, L., Papale, D., 2013. Simulation of grassland productivity by the combination of ground and satellite data. Agric. Ecosyst. Environ. 165, 163–172.
Mayaux, P., et al., 2006. Validation of theGlobal Land Cover 2000Map. IEEE Trans. Geosci. Remote Sens. 44 (7), 1728–1739.
Monteith, J.L., 1972. Solar radiation and productivity in tropical ecosystems. J. Appl. Ecol. 9, 747–766.
Moreno, A., Gilabert, M.A., Camacho, F., Martínez, B., 2013. Validation of daily global solar irradiation images from MSG over Spain. Renew. Energy 60, 332–342.
Moreno, A., García-Haro, F.J., Martínez, B., Gilabert, M.A., 2014. Noise reduction and gap filling of fAPAR series using an adapted local regression filter. Remote Sens. 6, 8238–8260. http://dx.doi.org/10.3390/rs6098238.
Myneni, R.B., Los, S.O., Asrar, G., 1995. Potential gross primary productivity of terrestrial vegetation from 1982-1990. Geophys. Res. Lett. 22, 2617–2620.
Nemani, R.R., Keeling, C.D., Hashimoto, H., Jolly, W.M., Piper, S.C., Tucker, C.J., et al., 2003. Climate-driven increases in global terrestrial net primary production from 1982 to 1999. Science 300, 1560–1563.
Papale, D., Valentini, R., 2003. A new assessment of European forests carbon exchanges by eddy fluxes and artificial neural network spatialization. Glob. Change Biol. 9, 525–535. http://dx.doi.org/10.1046/j.1365-2486.2003.00609.x.
Pastorello, G., et al., 2014. Observational data patterns for time series data quality assessment. e-Science (e-Science), 2014 IEEE 10th International Conference on, vol. 1, 271–278. http://dx.doi.org/10.1109/eScience.2014.45.
Quaife, T., Quegan, S., Disney, M., Lewis, P., Lomas, M., Woodward, F.I., 2008. Impact of land cover uncertainties on estimates of biospheric carbon fluxes. Global Biogeochem. Cycles 22. http://dx.doi.org/10.1029/2007GB003097.
Räsänen, M., et al., 2017. Carbon balance of a grazed savanna grassland ecosystem in South Africa. Biogeosciences 14, 1039–1054. http://dx.doi.org/10.5194/bg-14-1039-2017.
Roujean, J.L., Bréon, F.M., 1995. Estimating PAR absorbed by vegetation from bidirectional reflectance measurements. Remote Sens. Environ. 51, 373–384.
Running, S.W., Zhao, M., 2015. Daily GPP and Annual NPP (MOD17A2/A3) Products NASA Earth Observing System MODIS Land Algorithm. Useŕs Guide. Version 3.0 For Collection 6.
Running, S.W., Nemani, R.R., Heinsch, F.A., Zhao, M., Reeves, M., Hashimoto, H., 2004. A continuous satellite-derived measure of global terrestrial primary productivity: future science and applications. BioScience 56 (6), 547–560.
Sánchez-Ruiz, S., Moreno, A., Piles, M., Maselli, F., Carrara, A., Running, S., Gilabert, M.A., 2017. Quantifying water stress effect on daily light use efficiency in Mediterranean ecosystems using satellite data. Int. J. Digit. Earth 10 (6), 623–638.
Schaefer, K., et al., 2012. A model-data comparison of gross primary productivity: results from the North American Carbon Program site synthesis. J. Geophys. Res. 117, G03010. http://dx.doi.org/10.1029/2012JG001960.
Sepulcre, G., Vogt, J., Arboleda, A., Antofie, T., 2014. Assessment of the EUMETSAT LSA-SAF evapotranspiration product for drought monitoring in Europe. Int. J. Appl. Earth Obs. Geoinf. 30, 190–202.
Sjöström, M., et al., 2013. Evaluation of MODIS gross primary productivity for Africa using eddy covariance data. Remote Sens. Environ. 131, 275–286.
Tagesson, T., Fensholt, R., Cropley, F., Guiro, I., Horion, S., Ehammer, A., Ardö, J., 2015. Dynamics in carbon exchange fluxes for a grazed semi-arid savanna ecosystem in West Africa. Agric. Ecosyst. Environ. 205, 15–24. http://dx.doi.org/10.1016/j.agee.2015.02.017.
Tagesson, T., et al., 2016a. Spatiotemporal variability in carbon exchange fluxes across the Sahel. Agric. For. Meteorol. 226–227, 108–118.
Tagesson, T., et al., 2016b. Very high carbon exchange fluxes for a grazed semi-arid savanna ecosystem in West Africa. Danish J. Geogr. 116, 93–109.
Tagesson, T., et al., 2017. Modelling spatial and temporal dynamics of gross primary production in the Sahel from earth-observation-based photosynthetic capacity and quantum efficiency. Biogeosciences 14 (5), 1333–1348.
Tang, X., Li, H., Huang, N., Li, X., Xu, X., Ding, D., Xie, J., 2015. A comprehensive assessment of MODIS-derived GPP for forest ecosystems using the site-level FLUXNET database. Environ. Earth Sci. 74, 5907–5918. http://dx.doi.org/10.1007/s12665-015-4615-0.
Tian, H., Chen, G., Liu, M., et al., 2010. Model estimates of net primary productivity, evapotranspiration, and water use efficiency in the terrestrial ecosystems of the Southern United States during 1895–2007. For. Ecol. Manag. 259 (7), 1311–1327.
Tramontana, G., et al., 2016. Predicting carbon dioxide and energy fluxes across global FLUXNET sites with regression. Biogeosciences 13, 4291–4313. http://dx.doi.org/10.5194/bg-13-4291-2016.
Trigo, I.F., et al., 2011. The satellite application facility on land surface analysis. Int. J. Remote Sens. 32, 2725–2744. http://dx.doi.org/10.1080/01431161003743199.
Vörösmarty, C.J., Federer, C.A., Schloss, A.L., 1998. Potential evaporation functions compared on US watersheds: possible implications for global-scale water balance and terrestrial ecosystem modelling. J. Hydrol. 207, 147–169.
Valentini, R., et al., 2014. A full greenhouse gases budget of Africa: synthesis, uncertainties, and vulnerabilities. Biogeosciences 11, 381–407. http://dx.doi.org/10.5194/bg-11-381-2014.
Van Wijk, M.T., Bouten, W., 1999. Water and carbon fluxes above European coniferous forests modeled with artificial neural networks. Ecol. Mod. 120, 181–197.
Waring, H.R., Running, S.W., 2007. Forest Ecosystems Analysis at Multiples Scales, 3rd ed. Academic Press, San Diego.
Yang, F., et al., 2007. Developing a continental-scale measure of gross primary production by combining MODIS and AmeriFlux data through support vector machine approach. Remote Sens. Environ. 110, 109–122.
Yebra, M., Van Dijk, A.I.J.M., Leuning, R., Guerschman, J.P., 2015. Global vegetation gross primary production estimation using satellite-derived light-use efficiency and canopy conductance. Remote Sens. Environ. 163, 206–216. http://dx.doi.org/10.1016/j.rse.2015.03.016.
Zhao, M., Running, S.W., 2010. Drought-induced reduction in global terrestrial net primary production from 2000 through 2009. Science 329, 940–943.
Zhao, M., Running, S.W., Nemani, R.R., 2006. Sensitivity of Moderate Resolution Imaging Spectroradiometer (MODIS) terrestrial primary production to the accuracy of meteorological reanalyses. J. Geophys. Res. 111, G01002. http://dx.doi.org/10.1029/2004JG000004.
Zhao, M., Running, S.W., Heinsch, F.A., Nemani, R.R., 2011. MODIS derived terrestrial primary production. Land Remote Sensing and Global Environmental Change. Springer, New York, pp. 635–660. http://dx.doi.org/10.1007/978-1-4419-6749-7_28.